Simultaneous Estimation of Sample Surface Topography and Elasticity utilizing Contact–Mode AFM

Sakiya Watanabe and Hiroshi Fujimoto
Department of Electrical Engineering,
The University of Tokyo
5–1–5, Kashiwanoha, Kashiwa, Chiba, 277–8561, Japan
Telephone: +81–4–7136–3881
Fax: +81–4–7136–3881
Email: watanabe@hflab.k.u–tokyo.ac.jp, fujimoto@k.u–tokyo.ac.jp

***Abstract*—Atomic Force Microscope (AFM) is the device which can be applied to measure the surface topography of samples in nano–scale. Because the cantilever holds its physical contact with samples, it is also possible to measure elasticity of samples in principle. However, compared with the implovement of scanning performance, the technologies for viscosity and elasticity measurements are still underdeveloped. The proposal method measures the surface topography in forward scan (FWS) and the elasticity in backward scan (BWS). Furthermore, this paper introduces Surface Topography Observer (STO) and Perfect Tracking Control (PTC) in order to improve accuracy of the measurement.**

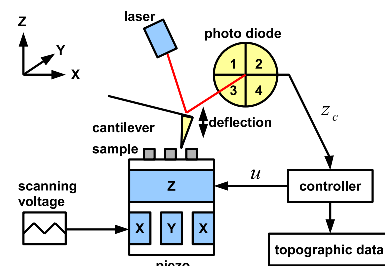

Fig. 1. Optical lever method (AFM).

I. Introduction

The rapid development of the atomic and molecular electronics contributes to the development of many fields like informatics, biotechnologies, etc. Atomic Force Microscope (AFM), which can measure the surface topography of samples in nano–scale, is one of the milestone products during this development.

Thanks to the feature of holding a physical contact with samples, AFM can detect atomic force between atoms. Therefore, unlike Scanning Tunneling Microscope (STM), whose samples should be conductive materials, AFM does not have much restriction on sample materials. Furthermore, AFM contributes to nano–manipulation because of broad utility [1]. For accuracy measurement, it is known that conventional feedback control methods result in time–consuming of measurement. In order to improve scanning speed and accuracy, many methods have been proposed from the view point of hardware and control theory [2]–[5]. The authors' research group has applied a learning control method as well as an observer on AFM, and fast and precise scanning control is obtained [6][7].

This paper deals with measuring the sample's elasticity using AFM. In many cases, material elasticity and viscosity are important information, especially when measuring soft materials like protein. In addition, it would be able to develop a new material if the characteristic of the sample is known. There are several studies on measuring the elasticity and viscosity of samples using AFM, for instance, analysis of the force–distance curve [8], or measuring of sample's elasticity by Recursive Least Square (RLS) method [9]. However, sample's elasticity and viscosity measurement technique has not been developed as the high speed scanning and high accuracy measurement techniques [10].

The authors' research group proposed the method which can measure sample's surface topography and elasticity in alternate shifts [11]. This method estimates elasticity of the sample using previous line sample surface topography. However, the resolution of this method is decreased by half because this method alternately measures surface topography and elasticity. In addition, the accuracy of the elasticity estimation would be degraded if the surface topography of present scanning line is quite different from the previous line.

For these problems, this paper proposes a new method which measures sample surface topography in forward scan (FWS), and estimates its elasticity in backward scan (BWS). This method increases the resolution and estimation error. Furthermore, this paper introduces Surface Topography Observer (STO) [6][7] and Perfect Tracking Control (PTC) [12] in order to improve the accuracy of the estimation.

II. Atomic Force Microscope

This section explains our experiment device. There are basically two types of AFM. One is contact–mode AFM, and the other is Dynamic–mode AFM. Contact–mode AFM can measure samples accurately, and its physical model is simpler than dynamic–mode AFM. This paper only considers contact–mode AFM.

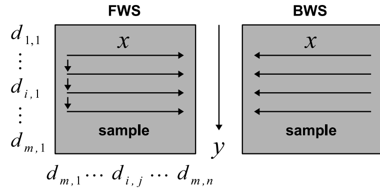

(a) Surface scan route of the cantilever.

	FWS				BWS			
N	1	2	$\cdots$	n	n	$\cdots$	2	1
Previous Line	$d_{i-1,1}$	$d_{i-1,2}$	$\cdots$	$d_{i-1,n}$	$d_{i-1,n}$	$\cdots$	$d_{i-1,2}$	$d_{i-1,1}$
Scanning Line	$d_{i,1}$	$d_{i,2}$	$\cdots$	$d_{i,n}$	$d_{i,n}$	$\cdots$	$d_{i,2}$	$d_{i,1}$

(b) Reverse disturbance of AFM.

Fig. 2. Scan route and surface topography.

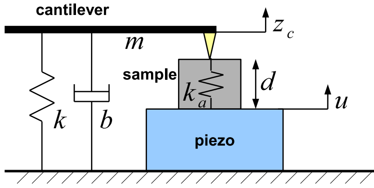

Fig. 3. Physical model of contact–mode AFM.

A. Contact–mode AFM

In general, there are two ways to measure the displacement of cantilever by surface topography. One is to measure the interference of laser beams (optical interferometry). The other is to measure the reflection angle of laser beam (optical lever method). This paper uses the optical lever method. As shown in Fig. 1, the change of optical strength is measured at photo diodes. The bend of the cantilever tip by the sample surface topography can be detected by the photo diodes, then compensated by feedback controller by moving piezo stage in Z–direction. Fig. 2 shows the surface scan route of the cantilever. The scan route consists of forward scan (FWS) and backward scan (BWS). In FWS, AFM scans the sample from left to right. In BWS, it scans the same route from right to left. The sample image is obtained by scanning in FWS and BWS repeatedly in Y–direction. The sample surface topography in the i line, j column is defined as d_{ij}.

B. Physical model of contact–mode AFM

This paper assumes that sample's viscosity can be neglected. Fig. 3 shows the physical model of contact–mode AFM, where m, b, k, d denote the mass, the viscosity coefficient, the spring constant of the cantilever, and the displacement of the surface topography respectively. k_a, z_c, and u denote the elasticity of the sample, the bend of the cantilever and input for piezo actuator in Z–direction, Thus, the motion equation of the cantilever is represented by

$$z_c = \frac{k_a}{ms^2 + bs + (k + k_a)}(u + d). \quad (1)$$

Without loss of generality, we assume that the spring constant of the sample is far smaller than that of the cantilever, i.e., $k_a \ll k$. Following this assumption, eq. (1) is rewritten as

$$z_c \simeq \frac{k_a}{ms^2 + bs + k}(u + d). \quad (2)$$

In the acutual AFM, there is a scale setting gain g when the displacement is detected by photo diodes. Transfer function of contact–mode AFM is rewritten as

$$P(s) = \frac{z_c}{u} = g\frac{k_a}{ms^2 + bs + k} = \frac{k'_a}{s^2 + b's + k'}, \quad (3)$$

where $k' = \frac{k}{m}$, $b' = \frac{b}{m}$, $k'_a = g\frac{k_a}{m}$.

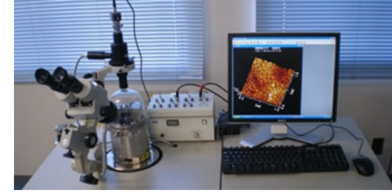

Fig. 4. Experimental device.

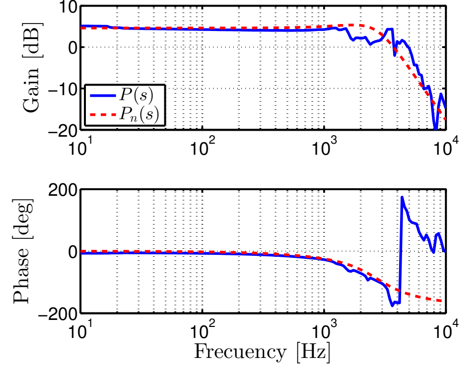

Fig. 5. Frequency responce of the Silicon sample.

C. Experimental setup

In our experimental setup, JSPM–5200 manufactured by JEOL Ltd. is customized as shown in Fig. 4. Our control algorithm is implemented and verified in a DSP–based–control–system.

We use the silicon sample for measurement. Fig. 5 shows the frequency response, which is the response from input u to the cantilever position z_c. According to Fig. 5, the nominal plant can be attained as

$$P_n(s) = \frac{5.07 \times 10^8}{s^2 + 1.90 \times 10^4 s + 2.98 \times 10^8}. \quad (4)$$

However, eq. (4) is obtained at one place. Usually, spring constant of the sample differs from one location to another. Therefore, accurate elasticity estimation at every point of samples is important.

This paper uses the analog phase–lag compensator used in commercial products

$$C_{\text{fb}}(s) = \frac{\omega_c}{s + \omega_c}k_p, \quad (5)$$

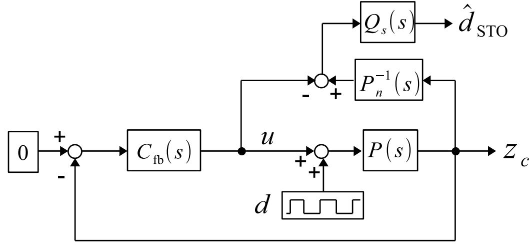

Fig. 6. Block diagram of STO.

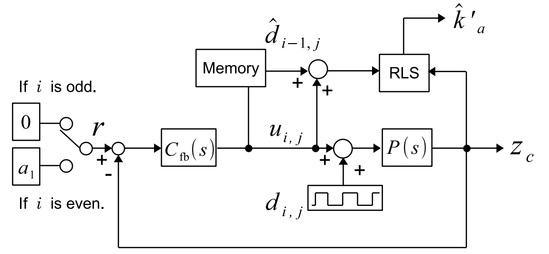

Fig. 7. Block diagram of the conventional method.

as the feedback controller, The parameters are tuned as $k_p = 100$, $\omega_c = 2\pi f_c$ ($f_c = 0.5$ Hz) based on the mannual of JSPM–5200.

III. CONTROL METHOD

A. Surface topography observer

The sample surface topography d can be estimated by disturbance observer from the control input $u(t)$ and the output $z_c(t)$. The block diagram of this observer is shown in Fig. 6, where $Q_s(s) = (\frac{\omega_s}{s+\omega_s})^2$ is a low–pass filter to make P^{-1} proper, and ω_s is 1000 rad/s. This special disturbance observer is named as the surface topography observer (STO). Because the STO is implemented as open loop observer, the bandwidth is not limited from the closed loop system, and the cut–off frequency of $Q_s(s)$ can be raised to near the Nyquist frequency.

B. Perfect tracking control

Perfect tracking control (PTC) consists of the 2–DOF control system [12]. The feedforward controller is designed as a stable inverse system of the plant by applying multirate control. In multirate feedforward controller, the control input is changed n times during one sampling period ($T_y = nT_u$), where n is the plant order. PTC method realizes perfect tracking to the reference at each sampling point. In addition, when there is disturbance or modeling error, tracking error is reduced by feedback controller.

From (3), the discrete–time plant $P[z]$ can be represented by

$$\begin{aligned} \boldsymbol{x}[k+1] &= \boldsymbol{A}_s\boldsymbol{x}[k] + \boldsymbol{B}_s u[k], && (6)\\ z_c[k] &= \boldsymbol{C}_s\boldsymbol{x}[k]. && (7)\end{aligned}$$

Therefore, the multirate discrete-time state equation can be represented by

$$\begin{aligned} \boldsymbol{x}[i+1] &= \boldsymbol{A}\boldsymbol{x}[i] + \boldsymbol{B}\boldsymbol{u}[i], && (8)\\ z_c[i] &= \boldsymbol{C}\boldsymbol{x}[i]. && (9)\end{aligned}$$

The coefficients are given by

$$\boldsymbol{A} = \boldsymbol{A}_s^2, \boldsymbol{B} = [\boldsymbol{A}_s\boldsymbol{B}_s,\ \boldsymbol{B}_s], \quad (10)$$

$$\boldsymbol{C} = 1, \boldsymbol{u}_{\text{ff}}[i] = \Big[u_1[i],\ u_2[i]\Big]^{\text{T}}. \quad (11)$$

when the plant is second-order system. Therefore, feedforward input is written as

$$\boldsymbol{u}_{\text{ff}} = \boldsymbol{B}^{-1}(\boldsymbol{I} - z^{-1}\boldsymbol{A})\boldsymbol{x}[i+1]. \quad (12)$$

C. Recursive least square

RLS is a method to identify parameters of system [13]. This subsection explains the algorithm of RLS.

Input–output relation is denoted by

$$\begin{aligned} y[k] + a_1 y[k-1] + \cdots + \quad a_{n_a} \quad y[k-n_a]\\ = b_1 u[k-1] + \quad \cdots \quad + b_{n_b} u[k-n_b]. \quad (13)\end{aligned}$$

This equation is rewritten as

$$y[k] = \boldsymbol{\theta}^{\text{T}}[k]\boldsymbol{\varphi}[k], \quad (14)$$

where $\boldsymbol{\theta}$ and $\boldsymbol{\varphi}$ are the unkown parameter vector and the regression vector defined as

$$\begin{aligned} \boldsymbol{\theta}[k] &= [\ a_1, ..., a_{n_a}, b_1, ..., b_{n_b}\ ]^{\text{T}}, && (15)\\ \boldsymbol{\varphi}[k] &= [-y[k-1], ..., -y[k-n_a], u[k-1], ..., u[k-n_b]]^{\text{T}}. && (16)\end{aligned}$$

The estimation of the unknown parameter vector $\boldsymbol{\theta}$ is denoted by

$$\begin{aligned} \hat{\boldsymbol{\theta}}[k] &= \hat{\boldsymbol{\theta}}[k-1] + \frac{\boldsymbol{P}[k-1]\boldsymbol{\varphi}[k]}{\lambda + \boldsymbol{\varphi}[k]^{\text{T}}\boldsymbol{P}[k-1]\boldsymbol{\varphi}[k]}\epsilon[k] && (17)\\ \epsilon[k] &= y[k] - \boldsymbol{\varphi}^{\text{T}}[k]\hat{\boldsymbol{\theta}}[k-1] && (18)\\ \boldsymbol{P}[k] &= \frac{1}{\lambda}\Big(\boldsymbol{P}[k-1] - \frac{\boldsymbol{P}[k-1]\boldsymbol{\varphi}[k]\boldsymbol{\varphi}^{\text{T}}[k]\boldsymbol{P}[k-1]}{\lambda + \boldsymbol{\varphi}^{\text{T}}[k]\boldsymbol{P}[k-1]\boldsymbol{\varphi}[k]}\Big) && (19)\end{aligned}$$

where λ is the forgetting factor ($0 \leq \lambda \leq 1$), $\hat{\boldsymbol{\theta}} = 0$ and $\boldsymbol{P}[0] = \gamma I$ ($\gamma > 0$).

IV. ELASTICITY ESTIMATION

A. Conventional method

This section introduces the conventional elasticity estimation method which uses the previous line surface topography [11]. Fig. 7 shows the block diagram of the conventional method.

In contact–mode AFM, the surface topography is measured by $u = -\hat{d} \simeq -d$. This paper assumes that the sample is satiny and the i th line (measuring point) is closed to the $(i-1)$ th line in FWS. That is

$$d_{i,j} \simeq \hat{d}_{i-1,j} = -u_{i-1,j}. \quad (20)$$

Therefore, eq. (3) is rewritten as

$$\begin{aligned} Q_r(s)\Big(s^2+b's+k'\Big)z &= Q_r(s)k'_a\Big(u_{i,j}+d_{i,j}\Big) \\ &\simeq Q_r(s)k'_a\Big(u_{i,j}-u_{i-1,j}\Big), \end{aligned} \tag{21}$$

where $Q_r(s) = \frac{\omega_r^2}{(s+\omega_r)^2}$ is the low–pass filter to make the left side of (21) proper. This equation is rewritten by (14), where

$$\theta = k'_a, \tag{22}$$

$$\varphi = Q_r(s)\Big(u_{i,j}-u_{i-1,j}\Big), \tag{23}$$

$$y = Q_r(s)\Big(s^2+b's+k'\Big)z_c. \tag{24}$$

From (3), the denominator coefficient of the transfer function is independent on spring constant of the sample k_a, when spring constant of sample is far smaller than that of the cantilever. Therefore, the following equation can be obtained.

$$b' = 1.90\times 10^4, \tag{25}$$

$$k' = 2.98\times 10^8. \tag{26}$$

Thus, we can estimate sample's spring k'_a and surface topography d using RLS method.

From (20), (23) is expressed by

$$\varphi = u_{i,j}-u_{i-1,j} \simeq 0. \tag{27}$$

In actual measurement, output is corrupted by noise. The S/N ratio is small when input signal is too small. Thus, such exact estimation results is obtained only when input signal is large. From Fig. 7, the S/N ratio is improved when a proper reference r is given. However, this means that the cantilever pushes a sample strongly. The material which needs elastic measurement is soft, hence, elastic deformation arises between them. Furthermore, the soft material may be destroyed by the force from the cantilever. Therefore, it is undesirable to have a reference with large magnitude.

In this conventional method, the reference r is changed from 0 to a_1 for every sequence. In this case, plant input u_i is expressed by

$$u_{i,j} = \frac{C_{\mathrm{fb}}}{1+PC_{\mathrm{fb}}}r - \frac{PC_{\mathrm{fb}}}{1+PC_{\mathrm{fb}}}d_{i,j}, \tag{28}$$

$$r = \begin{cases} 0 & \text{If } i \text{ is odd,} \\ a_1 > 0 & \text{If } i \text{ is even,} \end{cases} \tag{29}$$

where a_1 is the value not to cause too large elastic deformation. In this method, the S/N ratio can be improved, and the damage given to the sample is reduced.

B. Proposed method

The resolution of the conventional method decreases by half because it alternately measures surface topography and elasticity. Moreover, an estimation error occurs when the surface topography of the previous line is different from that of scanning line.

This section proposes the method which measures the sample surface topography in FWS, and estimates the sample elasticity in BWS. Furthermore, we introduces STO and PTC for more accurate estimation. Fig. 8 shows the diagram of this proposed method.

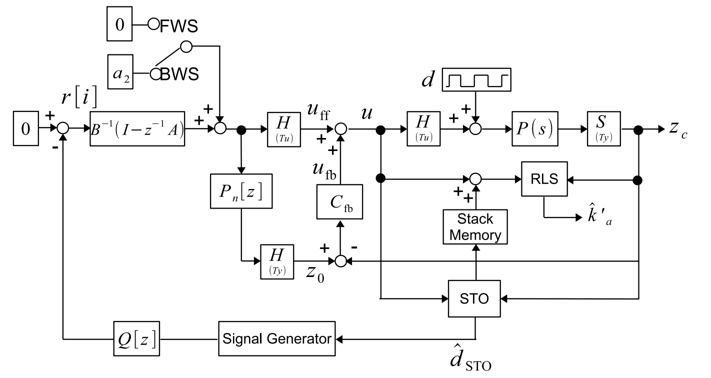

Fig. 8. Block diagram of the proposed method.

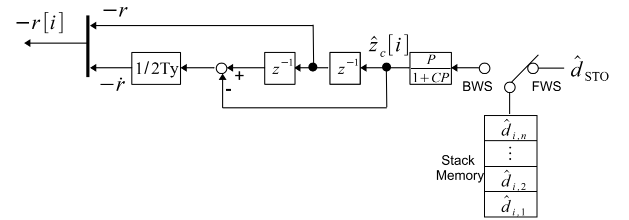

Fig. 9. Signal generator.

1) Signal generator: This subsection explains the signal generator (SG) for the perfect tracking to sample surface topography in BWS. State variables is defined by $\boldsymbol{x} = [z_c,\ \dot{z}_c]$. Then, the SG can generate the desired reference of velocity as $\dot{r}[i] = \frac{r[i+1]-r[i-1]}{2T_y}$.

In BWS, the reference for PTC is generated using the surface topography obtained in FWS, because the surface topography is regarded as a cyclic disturbance in FWS and BWS. However, surface topography in BWS is inverted in FWS as shown Fig. 2(b). The disturbance response in FWS differs from that in BWS because of the dynamics of the AFM plant and FB controller.

In this proposed method, the reference in BWS is obtained by

$$r = -\frac{P_n}{1+C_{\mathrm{fb}}P_n}\hat{d}_{\mathrm{STO}}, \tag{30}$$

where d_{STO} is the estimated surface topography in FWS. Fig. 9 shows the proposed signal generator, where $Q[z] = \left(\frac{z+2+z^{-1}}{4}\right)^2$ is the zero-phase low–pass filter for cutting noise.

2) Proposed elasticity estimation method: The proposed method measures the surface topography in FWS and estimates the sample elasticity in BWS. Fig. 8 shows the block diagram of the proposed method. In FWS, AFM is controlled by FB controller, and the surface topography estimated by STO is stored to the stack memory. In BWS, AFM tracks to the surface topography by PTC and estimates the sample elasticity using

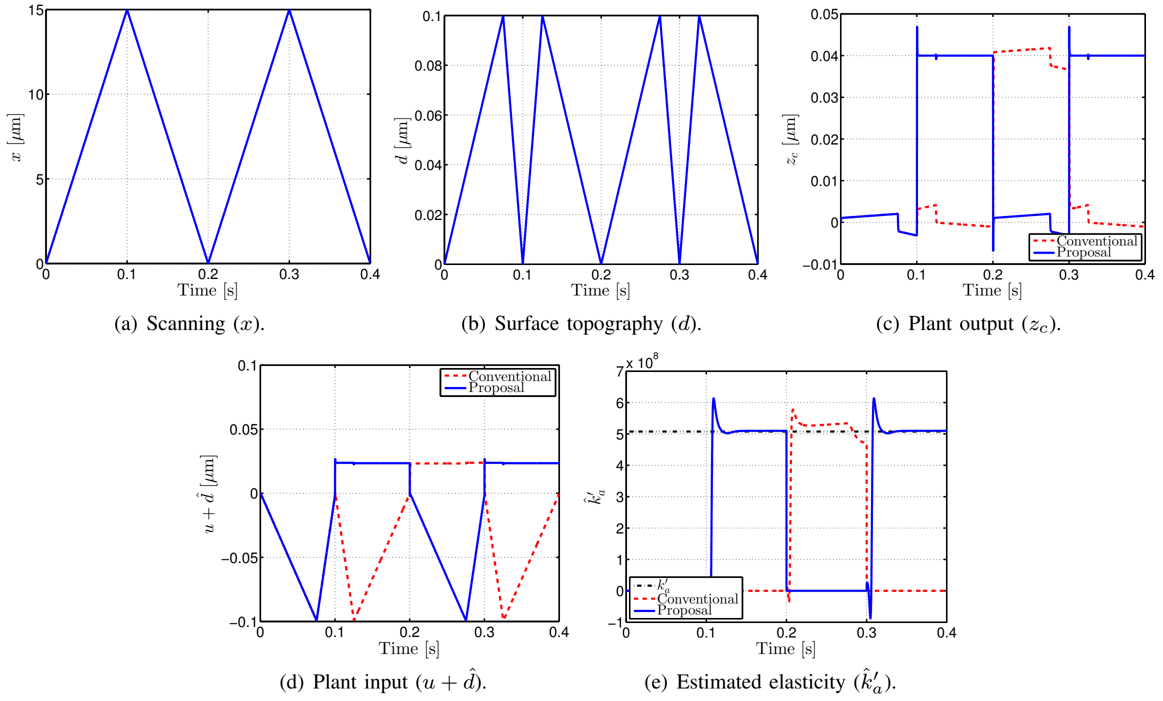

Fig. 10. Simulation results.

RLS method, where

$$\theta = k'_a, \tag{31}$$

$$\varphi = Q_r(s)\left(u + \hat{d}_{STO}\right), \tag{32}$$

$$y = Q_r(s)\left(s^2 + b's + k'\right)z. \tag{33}$$

Regression vector is denoted by

$$\varphi = Q_r(s)\left(u + \hat{d}_{STO}\right) \simeq 0, \tag{34}$$

because AFM can obtain perfect tracking of the surface topography in BWS. Therefore, the S/N ratio is too small just like the conventional method. In order to improve the S/N ratio, the proposed method adds a_2 to the control input. The response from a_2 to z_c is denoted by

$$z_c = \frac{P(1 + C_{\text{fb}}P_n)}{1 + PC_{\text{fb}}}a_2 \simeq Pa_2 \tag{35}$$

Thus, the S/N ratio can be improved and the more accurate estimation is realized.

The resolution of this method is doubled compared to the conventional. Moreover, an elasticity estimation error is improved because the cantilever scans the same route in FWS and BWS.

V. SIMULATION AND EXPERIMENTAL RESULTS

This section verifies the effectiveness of the proposed method by simulations and experiments.

A. Simulation results

This subsection verifies the effectiveness of the proposal method by simulation. This simulation uses the plant model as (4) in this simulation. Fig. 10 shows the simulation results. Fig. 10(a) shows a scanning route of the cantilever, where increase and decrease of the triangle wave represent FWS and BWS respectively. Fig. 10(b) shows the measured surface topography d. Fig. 10(c), 10(d) show the plant output z_c and estimated plant input $u + \hat{d}$. From Fig. 10(c), the conventional has a tracking error at $0.2 \sim 0.3$, when elasticity estimation. On the other hand, the proposed method realizes perfect tracking to surface topography at $0.1 \sim 0.2s$, $0.3 \sim 0.4s$ in BWS.

Fig. 10(e) shows the estimation results of sample's spring constant $\hat{k}'_a$. Although the conventional method estimates the elasticity at FWS in alternate shifts, the proposed method estimates at every BWS. Therefore, the elasticity is estimated at $0.1 \sim 0.2$ s, $0.3 \sim 0.4$ s in proposal, and at $0.2 \sim 0.3$ s in conventional. In other words, the resolution of the proposed method is doubled compared to the conventional.

In this simulation, the sample constant is obtained by $\hat{k}'_a = 5.07 \times 10^8$ from (4). The conventional method has an estimation error of elasticity. This is because the conventional method estimates the elasticity using $\hat{d} \simeq -u$, and dynamics of the plant and controller negatively affect to the estimation accuracy. However, the proposed method is more accurate in estimation than the conventional.

B. Experimental results

Fig. 11 shows experimental results using the silicon sample. Fig. 11(a) shows a scanning route of probe, where increase and decrease of the triangle wave represent FWS and BWS

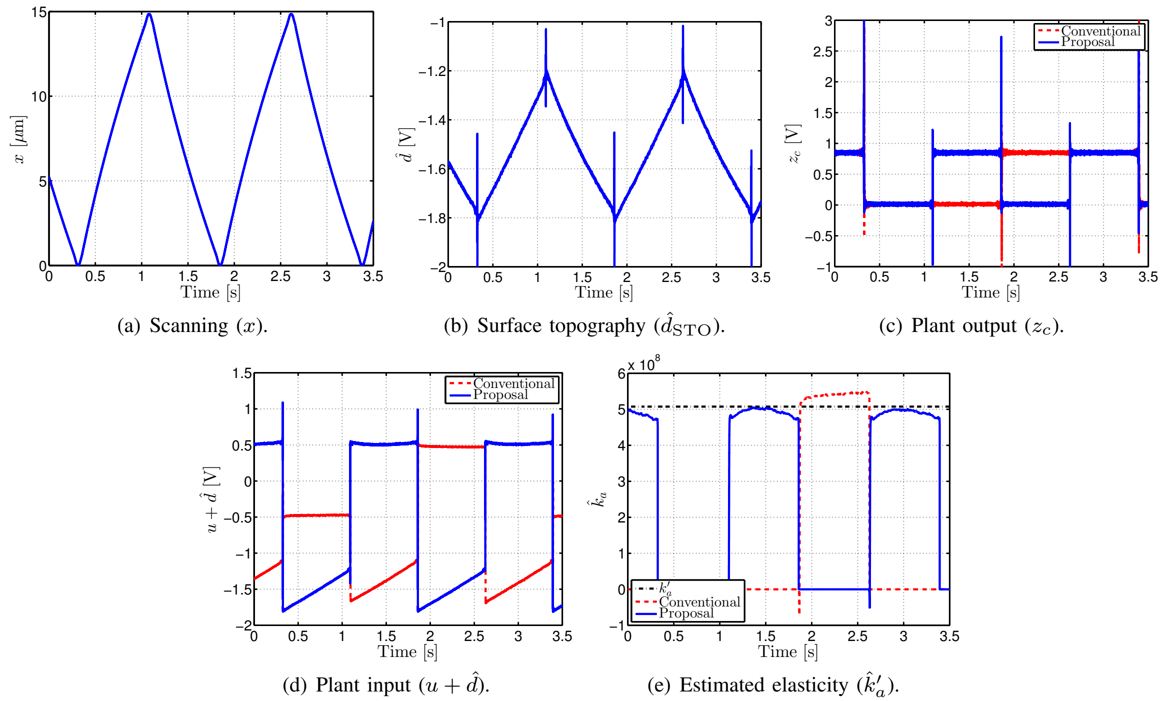

(a) Scanning (x).
(b) Surface topography ($\hat{d}_{\mathrm{STO}}$).
(c) Plant output (z_c).
(d) Plant input ($u + \hat{d}$).
(e) Estimated elasticity ($\hat{k}'_a$).

Fig. 11. Experimental results.

respectively. Fig. 11(b) shows the surface topography estimated by STO. Fig. 11(c), 11(d) show the plant output z_c and estimated input to the plant $u + \hat{d}$. Fig. 11(e) shows estimated sample's spring constant $\hat{k}'_a$. The elasticity is estimated at $1.1 \sim 1.8$ s, $2.6 \sim 3.4$ s in the proposal, and at $1.8 \sim 2.6$ s in the conventional. In this experiment, the silicon sample is clean and its elasticity should be constant at every scanning point. The proposed method can estimate more accurately than the conventional.

In proposed method, the accuracy of the estimated elasticity is degraded at $1.1 \sim 1.2$ s, $1.7 \sim 1.8$ s. This is because the surface topography estimated in FWS is different from the true surface topography.

VI. Conclusion

This paper proposed a new method to measure sample surface topography in FWS and estimate sample elasticity in BWS. This proposed method can obtain sample surface topography and elasticity by scanning the sample just one time. The effectiveness of the proposed method is also verified by simulations and experiments.

In future works, the elasticity estimation will be taken into account based on more precise model of AFM, considering sample's viscosity. Furthermore, it is necessary to extend our approach to dynamic–mode AFM, which can reduce the force to soft material.

References

[1] C. Onal, C. Pawasche, M. Sitti, "A scaled birateral control system for experimental 1–D teleoperated nanomanipulation applications", Intelligent Robots and Systems, pp. 483–488, 2007

[2] T. Ando, "Control Teqniques in High–speed Atomic Force Microscopy", American Control Conference, pp. 3194–3200, 2008

[3] A. Flemming, "A Method for Reduction Piezoelectric Non–Linearity in Scanning Probe Microscope Images", American Control Conference, pp. 2861–2866, 2011

[4] G. Schitter, P. Thurner, P. Hansma, "Design and input–shaping control of a novel scanner for high–speed atomic force microscopy", Mechatronics, Vol. 18, pp. 282–288, 2008

[5] L. Mahmood, S. Moheimani, "Improvement of accuracy and speed of a commercial AFM using positive feedback control", American Control Conference, pp. 973–978, 2009

[6] T. Shiraishi, H. Fujimoto, "High–Speed Atomic Force Microscope by Surface Topography Observer", Japanese Journal of Applied Physics, Vol. 51, pp. 026602–026602–7, 2012

[7] H. Fujimoto, T. Ohshima, "Contact–mode AFM Control with Modified Surface Topography Learning Observer and PTC", 34th Annual Conference of the IEEE Industrial Electronics Society, pp. 2515–2520, 2008

[8] K. Nakajima, S. Fujinami, D. Wang, T. Nishi, "Evaluation og Viscoelastic Properties of Polymeric Materials by Atomic Force Microscopy", Journal of the Japan Society of Colour Material, Vol. 83, pp. 108–144, 2010(in Japanese)

[9] D. Kim, J. Park, M. Kim, K. Hong, "AFM–based identification of the dynamic properties of globular protein : simulation study", Journal of Mechanical Science and Technology, Vol. 22, pp. 2203–2212, 2012

[10] "Roadmap of Elasticity Measurement by AFM", Japan Society for the Promotion Science nanoprobe technology 167 committee, 2012

[11] S. Watanabe, H. Fujimoto, "Estimation of Sample Elasticity Utilizing Previous Surface Topography by AFM", the 39th Annual Conference of the IEEE Industrial Electronics Society, pp. 6460–6465, 2013

[12] H. Fujimoto, Y. Hori, A. Kawamura, "Perfect Tracking Control Based on Multirate Feedforward Control with Generalized Sampling Periods", IEEE Transaction on Industrial Electronics, Vol. 48, No. 3, pp. 636–644, 2001

[13] H. Fujimoto, B. Yao, "Multirate adaptive robust control for discrete-time non-minimum phase systems and application to lineaar motors", IEEE/ASNE Journal of Mechatronics, Vol. 10, pp. 371–377, 2005